Royal Norwegian Council
for Scientific and Industrial Research
(NTNF)

NORSAR

NORSAR Scientific Report No. 2-91/92

Semiannual Technical Summary

1 October 1991 – 31 March 1992

Kjeller, May 1992

APPROVED FOR PUBLIC RELEASE, DISTRIBUTION UNLIMITED

7.5 Automatic phase association and event location using data from a network of seismic microarrays

Introduction

As the number of digital seismic stations around the world increases, it becomes more and more important to automate the data processing. Traditionally, the data processing has consisted of the following steps:

- Detection of phases at the individual stations.
- Extraction of parameters of the detected phases.
- Association of phases at the different stations to form events.
- Event location.

To be able to conduct automatic phase association and event location, initial identification and azimuth estimation of the detected phases are essential.

Using three-component data from NORESS and ARCESS, Suteau-Henson (1991) showed that P- and S-phases could be correctly classified from polarization attributes with a success rate of 82% for NORESS and 89% for ARCESS. P-wave azimuths at both stations were estimated with a standard deviation of 7-11°. At ARCESS, the S-wave azimuths had a standard deviation of 18-19°, although with a 180° ambiguity, whereas the scatter in the S-wave azimuths at NORESS were signifcantly larger (a standard deviation of 25° for L_g and 42° for S_n).

Riviere-Barbier et al. (1992) conducted a similar study using three-component data from the IRIS/IDA stations in the former USSR. The results obtained from analysis of these 4 stations did not quite match the results obtained for NORESS and ARCESS, mainly due to more complex geology near the receivers. In both studies referenced above, the large differences in the wave propagation characteristics between the different regions required that the phase identification criteria be developed individually for each three-component station.

Despite the documented performance of different three-component processing schemes, there are to our knowledge no sparse three-component network where phase detection, phase association and event location are conducted in a completely automatic mode. It has, however, been demonstrated that the information provided by individual seismic arrays permits automatic phase association and event location using a network of array stations. The precise azimuth and apparent velocity estimates provided by f-k analysis of the array sensors constrain the use of the detected phases in the phase association procedure. Utilizing this information, the ESAL algorithm of the Intelligent Monitoring System (IMS) (Bache et al., 1990) produces routinely both regional and teleseismic event locations, using data from the 4 regional arrays in northern Europe (ARCESS, FINESA, GERESS and NORESS). Based on a somewhat different approach, the generalized beamforming method (GBF) (Ringdal and Kværna, 1989) produces automatically a regional bulletin using the same detection data.

A study of data recorded at the NORESS array (Kværna and Ringdal, 1992) showed that by supplementing a three-component station with a very small vertical sensor three-element array with a typical aperture of 300 meters, reliable phase identification could be obtained. The quite stable apparent velocity and azimuth estimates produced by f-k analysis of the 4 vertical sensors of this microarray, indicates that data from a network of such microarrays can be processed using existing phase associaton and event location algorithms.

In this contribution we will first evaluate the performance of microarrays at the ARCESS and FINESA sites. Although a separate study has been conducted at NORESS (Kværna and Ringdal, 1992), we will for comparison reevaluate the performance of a microarray at NORESS. Secondly, we will conduct network phase associaton and event location applying the GBF method to microarray data from ARCESS, FINESA and NORESS, see Fig. 7.5.1.

Microarrays

For all three microarrays we conducted automatic detection processing and post-detection analysis for a period of 12 days (9-20 April 1992). The detection processing was similar to that used in the study of Kværna and Ringdal (1992).

The post-detection processing included broadband f-k array analysis (Esmersoy et al., 1985; Kværna and Doornbos, 1986) of each detected signal using the 4 vertical-component sensors of the microarrays. For the f-k analysis, we used a 5 sec. long data interval starting 0.5 sec. before the estimated onset time, and a frequency band similar to the filter band of the detecting beam.

To obtain a data base against which to evaluate our results, we extracted all seismic phases detected by the three full arrays and associated with regional events for the 12-day period. Results from the generalized beamforming procedure (GBF) (Ringdal and Kværna, 1989) were used in order to validate these reference events. *P*-coda detections and multiple *S*-phases were ignored, so that each event provided a maximum of 3 phases (*P*, *S* and L_g). These phases were then matched to the detection lists produced by the microarrays, and the apparent velocity and azimuth estimates were compared.

The problem of false alarms is inevitably encountered when a detector is operated at a low detection threshold. In conducting automatic phase association and location it is critical to identify these false alarms. When processing the full arrays, phases with low apparent velocities (< 3.0 km/s) are generally discarded from further analysis. As the final step in the analysis of the individual microarrays, we evaluated their capability to identify phases with low apparent velocities. This was done by matching all detections of the microarray (both associated and unassociated phases) to the full array detection list, using the apparent velocitiy estimates of the full array as the reference.

ARCESS

The geometry of the ARCESS microarray is given in Fig. 7.5. 2. The center instrument A0 is three-component, whereas A1-A3 are vertical only. The aperture is about 300 meters.

Fig. 7.5.3 shows the apparent velocity estimates derived from vertical sensors of the microarray for *P* phases (circles) and *S* phases (asterisks) for the reference data set of phases associated with regional events. Of the 303 phases analyzed, 79.2% were correctly classified as *P* or *S* when an apparent velocity of 5.8 km/s was used to separate the two classes. These results are not as good as those earlier published for the NORESS site (Kværna and Ringdal, 1992), where a success rate exceeding 95% was found. It is particularly significant that for epicentral distances less than 600 km, several P-phases have S-type apparent velocities on the microarray. It is most likely that this phenomenon is due to the near-receiver structure, although no studies have been conducted to map the structure in any detail.

We have attempted to improve the initial phase identification by adding an additional constraint on the parameter data. We have observed that due to the preceding *P*-coda, the *S*-phases have seldom a high signal-to-noise ratio (SNR), whereas many of the *P* phases have high SNR. Based in these observations the following rule was introduced:

Phases with SNR > 10 and apparent velocity > 4.5 km/s are P-phases.

This improved the percentage of correctly classified phases to 84.8%.

In this study we have not attempted to include any three-component polarization attributes in the initial phase identification, but tried to evaluate what can be achieved using only f-k analysis of the 4 vertical sensors. As mentioned in the introduction, Suteau-Henson (1991) showed that by using three-component data from ARCESS, *P*- and *S*-phases could be correctly classified with a success rate of 89%. This indicates that if we combine the polarization attributes derived from the three-component instrument of the microarray with the attributes derived by f-k analysis of the 4 vertical sensors, there may be a significant improvement in the number of correctly classified phases.

Figs. 7.5.4 and 7.5.5 show a comparison between the azimuth estimates computed by f-k analysis of the microarray and the azimuth to the epicenters of the reference data set (computed by the GBF algorithm), for *P* and *S*-phases, respectively. For the *P*-phases of Fig. 7.5.4 the median error is 10.4^{o} and for the *S*-phases of Fig. 7.5.5 the median error is 6.8^{o}. These results show that azimuth constraints can be actively used in the phase association and event location procedure.

As the final step in the evaluation of the ARCESS microarray we estimated its capability to identify noise detections (false alarms). The reference data here were all detections of the full array where the f-k spectra showed typical signal behavior with a pronounced peak. The results are presented in Table 7.5.1a. From this table it is seen that 75.4% of the evaluated detections were correctly classified applying broadband f-k analysis to the microarray data.

For the 303 phases verified to be associated with regional events, a similar statistics is given in Table 7.5.1b. The important information in this table is that no associated phases are interpreted by the microarray as noise-detections (an apparent velocity of 3.2 km/s is used to determine the upper bound on the class of noise detections). From Tables 1a and 1b it can thus be concluded that for the data set considered, 36.3% of all microarray detections at ARCESS can be discarded from the automatic phase association and event location processing without classifying any verified regional phases as noise.

FINESA

The geometry of the FINESA microarray is given in Fig. 7.5.6. The sensors A1-A3 make an aperture of about 500 meters. The vertical component instrument A0 is not located at the center of the triangle, but is still the only candidate for a center instrument in the microarray. The three-component instrument is located at A1.

Fig. 7.5.7 shows the apparent velocity estimates derived from the four vertical sensors of the microarray or *P* phases (circles) and *S* phases (asterisks) for the reference data set of phases associated with regional events. Of the 355 phases analyzed, 78.6% were correctly classified as *P* or *S* when an apparent velocity of 5.8 km/s was used to separate the two classes. This is close to the success rate obtained for the ARCESS microarray. The majority of the events in the reference data base are found in the active mining areas in Estonia and western Russia, in a distance range between 150 and 250 km from the FINESA site. This is clearly seen on Fig. 7.5.7.

Another feature of Fig. 7.5.7 is the occurence of *P*-phases with very low apparent velocities in the same 150-250 km distance range. By comparing Figs. 7.5.6 and 7.5.2 we find that the aperture of the FINESA microarray is about 200 meters larger than the aperture of the ARCESS microarray. When processing local and regional phases with high dominant frequencies at the FINESA microarray, broad-band f-k analysis will suffer from spatial aliasing and the lack of coherency between the sensors, and some *P*-phases will therefore come out with low apparent velocities. We can overcome this problem by lowering the frequency band for f-k analysis or alternatively reduce the sensor spacing, but such steps have not been taken in this study. Note that for distances exceeding 400 km, the separation between *P* and *S*-phases are excellent.

Fig. 7.5.8 and Fig. 7.5.9 show a comparison between the azimuth estimates computed by f-k analysis of the microarray and the azimuth to the epicenters of the reference data set (computed by the GBF algorithm), for *P* and *S*-phases, respectively. For the *P*-phases of Fig. 7.5.8 the median error is 13.4^0 and for the *S*-phases of Fig. 7.5.9 the median error is 8.5^0. This is more than observed at the ARCESS array. The apparent alignment of *P*-wave azimuth estimates at about 150^0 (see Fig. 7.5.8) is also related to the problem with the lack of coherency and spatial aliasing at high frequencies. For such phases the f-k analysis often results in a low apparent velocity and an azimuth close to 150^0.

In Table 7.5.2a we present results from analysis of all detections at the FINESA microarray for the 12-day period. As for ARCESS we used the all full array detections where the f-k spectra showed typical signal behavior with a pronounced peak. 70.1% of the microar-

ray detections were correctly classified, which is less than at ARCESS. For the 355 phases verified to be associated with regional events a statistics similar to that of Table 7.2.1b is given in Table 7.5.2b. Both Tables 7.5.2a and 7.5.2b show that a significant number of *P*- and *S*-phases obtain low apparent velocities from f-k analysis of the microarray. This implies that if we were to discard detections with low apparent velocities from further analysis, we would also miss some of the real *P*- and *S*-phases, and that the total benefit from discarding the low-velocity detections in the case of FINESA is very moderate.

NORESS

Although the performance of a microarray at NORESS has been evaluated in a separate study (Kværna and Ringdal, 1992), we will for comparison reevaluate its capability using the common 12-day data set. Fig. 7.5.10 shows the geometry of the NORESS microarray, which is similar to that of ARCESS.

Fig. 7.5.11 shows the apparent velocity estimates derived from the 4 vertical sensors of the microarray for *P* phases (circles) and *S* phases (asterisks) for the reference data set of phases associated with regional events. Of the 164 phases analyzed, 93.3 % were correctly classified as *P* or *S* when an apparent velocity of 6.0 km/s was used to separate the two classes. This confirms the results of the study of (Kværna and Ringdal, 1992).

Figs. 7.5.12 and 7.5.13 show a comparison between the azimuth estimates computed by f-k analysis of the microarray and the azimuth to the epicenters of the reference data set (computed by the GBF algorithm), for *P* and *S*-phases, respectively. For the *P*-phases of Fig. 7.5.12 the median error is 14.0^0 and for the *S*-phases of Fig. 7.5.13 the median error is 6.5^o.

Table 7.5.3a gives results from analysis of all detections at the NORESS microarray for the 12-day period. 77.0% of the microarray detections were correctly classified, which is somewhat less than the percentage obtained by Kværna and Ringdal (1992). 11.2% of the detections were classified as noise which is significantly less than the percentage obtained by Kværna and Ringdal (1992). This difference can be explained by a difference in the noise field, as there are time intervals at NORESS when the number of detections with low apparent velocity increases substantially due to increased water flow and industrial activity in the nearby regions (Kværna, 1990). As was done for the other two microarrays we alse computed a statistics for the phases verified to be associated with regional events. We find from Table 7.5.3b that only one of the associated phases is interpreted as noise when an apparent velocity of 3.2 km/s is used as the upper bound on the class of noise detections.

Summary

We have found that seismic microarrays at the ARCESS and FINESA sites do not match the NORESS microarray performance in separating *P*- and *S*-phases based on the apparent velocity estimates. The percentage of correctly classified regional phases were for ARCESS 79.2%, for FINESA 78.6% and for NORESS 93.3%. The success rate for ARCESS was increased to 84.8% when an additional constraint based on SNR and apparent velocity was placed on the definition of *P*-phases. No attempt has been made to

include three-component data or context-sensitive information in the initial phase identification, although the potential for improvement is significant (Suteau-Henson, 1991, Riviere-Barbier et al., 1992).

A summary of the different success rates and median errors is given in Table 4. For direct comparison with the results of Riviere-Barbier et al. (1992), we have also included the percentage of phases with azimuth differences within 25^{o}.

The simple procedure of using apparent velocity estimates to classify *P*- and *S*-phases is very different from the complex classification criteria used at three-component stations (Suteau-Henson, 1991, Riviere-Barbier et al., 1992). For the three microarrays analyzed, almost the same classification criterion could be applied to each site. The only difference was that at NORESS an apparent velocity of 6.0 km/s ws used to separate *P* and *S*, whereas at ARCESS and FINESA 5.8 km/s was used. This indicates that at microarrays, very little data and data analysis is required to make initial phase identification work properly. In the two studies of three-component data referenced above it was found that the polarization characteristics of seismic phases were strongly site dependent, and that consequently an extensive data set had to be collected at each station in order to find usable criteria for initial phase identification.

The topic for the next section is to test whether the results presented above are of sufficient merit to allow reliable, automatic phase association and event location using data from a network of microarrays.

Phase association and event location using microarray data

We will in this work apply the generalized beamforming (GBF) method (Ringdal and Kværna, 1989) for associating phases and locating regional events using the detections from the three microarrays. The method is currently in routine use at NORSAR for processing data from the 4 regional arrays in northern Europe (ARCESS. FINESA, GERESS and NORESS), and our attempt will be to process the microarray data without introducing major changes in the processing parameters of the now operational version of the GBF algorithm. For details on the method we refer to a documentation report now in progress. However, we will in the following briefly outline the basic principles.

The GBF algorithm

The basic idea behind the GBF method is to associate detected phases to form seismic events by counting the number of phases that match a hypothetical event at a given target (beam) location at a given origin time. In order to avoid interfering phases that do not belong to the event in question, we impose constraints as part of the phase matching process. The most important constraints of the current operational GBF method are the following:

- Constraint on phase type (*P*, *S* and *noise*) based on apparent velocity estimates.
- Constraint on azimuth to epicenter from actual phase azimuth estimates.

- Constraint on distance to epicenter inferred from values of apparent velocity and dominant frequency.
- Constraint on the allowable phase type based on the pattern of phase and coda detections for local and regional events.
- Constraint on distance to epicenter from the pattern of *P*- and *S*-phases for local and regional events.

When processing the microarrays with the GBF method, we only introduced one single modification to the current operational GBF parameters. This was by adding the possibility of redefining *S*-phases to *P*- phases at ARCESS (see section on the ARCESS microarray). We might as well have tuned the GBF parameters more specifically towards processing microarrays, but as one of our intentions was to check the robustness of the GBF algorithm, we initially avoided such fine tuning.

Reference events

The events declared by the GBF algorithm from processing of the full regional arrays ARCESS, FINESA and NORESS were used as a reference data base for the 12 day period (9-20 April 1992). The GBF output was manually checked for inconsistencies, and false events were removed. This resulted in 428 reference events, and those with magnitude above 1.5 are shown on the map of Fig. 7.5.14. Note the large number of mining explosions on the Kola peninsula and in Estonia. The magnitudes M_L were computed using the formula of Båth (1981), and in the cases where several arrays detected *S*-phases, the magnitudes were averaged.

The reference locations should be used with caution, as the event waveforms have not been interactively analyzed.

Event detectability

As a definition of a reference event found by GBF processing of the microarray network we have used the following criterion:

If the difference in event location is less than 400 km and the difference in origin time is less than 120 seconds, the event is declared as detected by the microarray network.

The motivation behind using such wide acceptance limits is that all of these events will be flagged as candidates for subsequent interactive analysis, such that errors in phase association and timing of the detected phases can be corrected by the analyst.

Fig. 7.5.15 illustrates the event detectability as a function of distance to the closest array. Detected events are marked as stars, whereas non-detected events are shown by circles. A total number of 261 events (61%) were found by the microarray network. It is seen that beyond 600 km, no event with magnitude less than 2.0 is detected, whereas just below this distance limit events close to magnitude 1.0 are detected. We will therefore in the following proceed with a detectability study for events within 600 km of the closest array. Having the the map of Fig. 7.5.14 in mind, this constitute a geographical region covering a

triangle with the three microarrays in the corners extended by a circle sector of 600 km radius around each microarray. An area as defined above will also be the typical size of a region of interest for possible future microarrays.

A maximum likelihood estimation of event detectability (Ringdal, 1975) of the region defined above is presented in Fig. 7.5.16. From the number of detections/no detections at each magnitude, the 50% and 90% incremental detection thresholds are inferred. The 90% threshold is about $M_L = 1.8$, whereas the 50% threshold is found to be about $M_L = 0.8$. These numbers are further confirmed by comparing with the seismic bulletin of the University of Helsinki, Finland.

For an event to be defined by the GBF algoritm, a minimum of two defining phases are required. This might be, for example, a *P* and an *S* at one array or two *P*-phases at two arrays. In the previous section discussing the performance of each microarray, we found that a significant number of seismic phases were discarded from GBF processing due to erroneous estimates of apparent velocity and azimuth. In such cases where the azimuth or apparent velocity estimates fall outside the allowable range for GBF processing, it will often happen that a coda detection is used as a defining phase. This exploitation of redundant detections is one of the strong features of the GBF algorithm leading to the good event detectability of the microarray network, although the phase associations and the corresponding event location will not always be perfect.

Location differences

For 249 microarray events located within 600 km of the closest array, a histogram of the location difference between the microarray network and the full array network is given in Fig. 7.5.17. The median difference of the population is 47.4 km. The causes of the location differences can be divided into three types:

1. Differences in estimates of phase arrival times.
2. Use of coda phases as defining phases.
3. Occasionally, erroneous phase association.

Type 1 and 2 will in most cases result in minor to modest location differences, whereas type 3 often will cause large deviations.

By dividing the population into events with the same number of associated phases (microarray network), we obtain the distribution of Table 5. It is seen that the differences are generally reduced when the number of associated phases increase. This is due to the fact that the likelihood of erroneous phase association (type 3) is reduced when the number of associated phases increase.

False events

In practical operation of any phase association and event location algorithm, it is essential that the number of false events is kept at a moderate level. Our experience with the GBF algorithm applied to the full array network is that the number of false events is rather low.

A false alarm rate of 26% is found for the automatic GBF algorithm applied to the microarray network (see Table 7.5.6), which is a number that does not present a problem in an analyst review situation. No event with more than 3 associated phases (irrespective of number of arrays) were false (see Table 7.5.7), and the vast majority of the false events were one-array events with two defining phases (a *P* and an *S*-phase). From Table 7.5.8 it is clearly seen that most of the false 1-array events were found at the FINESA array. This is in accordance with our finding that the FINESA microarray had the lowest success rate in classifying *P* and *S*- phases from apparent velocity estimates.

Summary

It has been demonstrated that information derived from a sparse network of seismic microarrays (interstation distance ~ 1000 km) permits successful automatic phase association and regional event location using the GBF algorithm. The apparent velocity and azimuth estimates of the detected phases found by f-k analysis of the 4 vertical-component sensors of each microarray place strong constraints on the use of the detected phases. This enables subsequent GBF processing of the detection data to be performed with good event detectability combined with a low number of false events.

Although the initial phase identification based of the apparent velocity estimates from time to time resulted in mis-classification of the phases, the robustness of the GBF algorithm prevented events from being missed. The robustness was also accentuated by the fact that except for one change, the microarray network could be processed with the same parameter settings as the full array network.

For 249 events located within 600 km of the closest array, the median difference between automatic locations by the full array network and by the microarray network was only 47.4 km.

Information from the three-component sensors of the microarrays has not been used in this study, but the work of Suteau-Henson (1991) and Riviere-Barbier et al. (1992), indicate that further improvements in event detectability, correctness of phase association and consequently in event location can be achieved if this information is utilized.

Out of the 353 events formed after automatic GBF processing of the microarray network, only 92 (26%) were found to be false, a number that is easily handled in an analyst review situation. All events with 4 or more defining phases were real. The vast majority of the false events were associated with detections at the FINESA array.

In order to handle the large data volumes produced by modern digital seismic networks, a high degree of automated processing is essential. We have in this work shown that in Fennoscandia a sparse network of microarrays allows for such automated processing. Very little data collection and data analysis needs to be done to tune the parameters for the

algorithms for automatic phase association and event location. The Fennoscandian Shield constitutes a rather simple and homogeneous geological province, and it would therefore be if interest to investigate microarray performances in more complex geological environments.

T. Kværna

References

Bache, T., S. R. Bratt, J. Wang, R.M. Fung, C. Kobryn and J. W. Given (1990), The Intelligent Monitoring System, Bull. Seism. Soc. Am., 80, Part B, 1833-1851.

Båth, M. (1981): Local magnitude-recent research and current trends, Earth-Science Rev., 17, 315-398.

Esmersoy, L., V. F. Cormier and M. N. Toksöz (1985). Three component array processing, In The VELA Program, A. U. Kerr, Editor, Defence Advanced Research Projects Agency, Executive Graphics Services.

Kværna, T. (1990): Sources of short-term fluctuations in the seismic noise level at NORESS, Phys. Earth. Planet. Inter., 63, 269-276.

Kværna, T. and D.J. Doornbos (1986): An integrated approach to slowness analysis with arrays and three-component stations, Semiann. Tech. Summary, 1 October 1985-31 March 1986, NORSAR Sci. Rep. No 2- 85/86, Kjeller, Norway.

Kværna, T. and F. Ringdal (1992): Integrated array and three-component processing using a seismic microarray, Bull. Seism. Soc. Am., 82, 870-882.

Ringdal, F. and T. Kværna (1989): A multi-channel processing approach to real-time network detection, phase association, and threshold monitoring, Bull. Seism. Soc. Am., 79, 1927-1940.

Ringdal, F. (1975): On the estimation of seismic detection thresholds, Bull. Seism. Soc. Am., 65, 1631-1642.

Riviere-Barbier, F., A. Suteau-Henson, V.Z. Ryaboy and J.A. Carter (1992): Analysis of three-component data from IRIS/IDA stations in USSR, Bull. Seism. Soc. Am., 82, 192-220.

Suteau-Henson, A. (1991): Three-component analysis of regional phases at NORESS and ARCESS: Polarization and phase identification, Bull. Seism. Soc. Am., 81, 2419-2440.

	Classified as:		
Correct phase id (full array)	P (vel>5.8m/s)	S or Lg (3.2<vel≤5.8 km/s)	Noise (vel≤3.2 km/s)
P (vel>5.8)	343 (22.6%)	118 (7.8%)	58 (3.8%)
S or Lg (3.0<vel≤5.8 km/s)	109 (7.2%)	365 (24.0%)	55 (3.6%)
Noise (vel≤3.0 km/s)	6 (0.4%)	28 (1.8%)	439 (28.9%)

Total number of microarray detections evaluated: 1521
Total number of phases correctly classified: 1147 (75.4%)

Table 7.5.1a. All detections of the ARCESS microarray have been used as the basis for this statistics. The detections are classified based on estimated apparent velocities applying broadband f-k analysis to the vertical components of the microarray and "correct" phase identification is based on f-k results from the full ARCESS array.

	Classified as:		
Correct phase id	P (vel>5.8m/s)	S or Lg (3.2<vel≤5.8 km/s)	Noise (vel≤3.2 km/s)
P (from GBF)	86 (28.4%)	47 (15.5%)	0 (0.0%)
S or Lg (from GBF)	16 (5.3%)	154 (50.8%)	0 (0.0%)
Noise (none)	0 (0.0%)	0 (0.0%)	0 (0.0%)

Total number of phases evaluated: 303
Total number of phases correctly classified: 240 (79.2%)

Table 7.5.1b. In this table we have used the phases (*P*, *S* or L_g) verified to be associated with regional events as the "correct" phase identification, and the phases were classified based on estimated apparent velocities applying broadband f-k analysis to the vertical components of the ARCESS microarray.

	Classified as:		
Correct phase id (full array)	P (vel>5.8m/s)	S or Lg (3.2<vel≤5.8 km/s)	Noise (vel≤3.2 km/s)
P (vel>5.8)	385 (31.4%)	70 (5.7%)	42 (3.4%)
S or Lg (3.0<vel≤5.8 km/s)	42 (3.4%)	370 (30.2%)	172 (14.0%)
Noise (vel≤3.0 km/s)	5 (0.4%)	35 (2.9%)	104 (8.5%)

Total number of microarray detections evaluated: 1225
Total number of phases correctly classified: 920 (70.1%)

Table 7.5.2a. All detections of the FINESA microarray have been used as the basis for this statistics. The detections are classified based on estimated apparent velocities applying broadband f-k analysis to the vertical components of the microarray and "correct" phase identification is based on f-k results from the full FINESA array.

	Classified as:		
Correct phase id	P (vel>5.8m/s)	S or Lg (3.2<vel≤5.8 km/s)	Noise (vel≤3.2 km/s)
P (from GBF)	121 (34.1%)	16 (4.5%)	23 (6.5%)
S or Lg (from GBF)	12 (3.4%)	158 (44.5%)	25 (7.0%)
Noise (none)	0 (0.0%)	0 (0.0%)	0 (0.0%)

Total number of phases evaluated: 355
Total number of phases correctly classified: 279 (78.6%)

Table 7.5.2b. In this table we have used the phases (P, S or L_g) verified to be associated with regional events as the "correct" phase identification, and the phases were classified based on estimated apparent velocities applying broadband f-k analysis to the vertical components of the FINESA microarray.

	Classified as:		
Correct phase id (full array)	P (vel>6.0m/s)	S or Lg (3.2<vel≤6.0 km/s)	Noise (vel≤3.2 km/s)
P (vel>6.0)	260 (39.9%)	13 (2.0%)	9 (1.4%)
S or Lg (3.0<vel≤6.0 km/s)	51 (7.8%)	185 (28.4%)	7 (1.1%)
Noise (vel≤3.0 km/s)	12 (1.8%)	58 (8.9%)	57 (8.7%)

Total number of microarray detections evaluated: 652
Total number of phases correctly classified: 502 (77.0%)

Table 7.5.3a. All detections of the NORESS microarray have been used as the basis for this statistics. The detections are classified based on estimated apparent velocities applying broadband f-k analysis to the vertical components of the microarray and "correct" phase identification is based on f-k results from the full NORESS array.

	Classified as:		
Correct phase id	P (vel>6.0m/s)	S or Lg (3.2<vel≤6.0 km/s)	Noise (vel≤3.2 km/s)
P (from GBF)	70 (42.7%)	2 (1.2%)	0 (6.5%)
S or Lg (from GBF)	8 (4.9%)	83 (50.6%)	1 (0.6%)
Noise (none)	0 (0.0%)	0 (0.0%)	0 (0.0%)

Total number of phases evaluated: 164
Total number of phases correctly classified: 153 (93.3%)

Table 7.5.3b. In this table we have used the phases (P, S or L_g) verified to be associated with regional events as the "correct" phase identification, and the phases were classified based on estimated apparent velocities applying broadband f-k analysis to the vertical components of the NORESS microarray.

	ARCESS	FINESA	NORESS
Percentage of correctly classified phases	79.2% (84.8%)	78.6%	93.3%
Median azimuth error for P-phases	10.4°	13.4°	14.0°
Percentage of P-phases within 25°	78.5%	73.0%	86.1%
Median azimuth error for S-phases	6.8°	8.5°	6.5°
Percentage of S-phases within 25°	98.2%	88.0%	94.6%
Percentage of all detections classified as noise	36.3%	26.0%	11.2%
Percentage of verified phases classified as noise	0.0%	13.5%	0.6%

Table 7.5.4. This table contain a summary of the success rates for initial phase identification and the median errors in the azimuth estimates of the three microarrays considered. We have also included the percentage of P and S-phases with azimuth differences within 25^0 of the reference azimuth. Note that f-k analysis of the 4 vertical sensors of the microarrays is the only method being used to obtain these results.

	Number of defining phases (microarray network)						
	2	3	4	5	6	7	8
Number of events	144	53	23	14	9	3	3
Median location difference (km)	55.3	47.4	47.3	33.7	45.3	37.6	0.0
Median magnitude M_L	1.17	1.47	2.10	2.33	2.26	2.53	2.50

Table 7.5.5. After dividing the events into classes based on the number of defining phases, we give for each class the number of events, median location difference to the full network location and the median magnitude. Note that the location differences are generally reduced when the number of associated phases increase.

Declared events	Real events	False events
353	261 (74.0%)	92 (26.0%)

Table 7.5.6. Distribution of real and false events for the 353 events declared after GBF processing of the microarray network.

	1 array	2 arrays	3 arrays
2 associated phases	62	18	-
3 associated phases	3	7	2

Table 7.5.7. Distribution of detecting arrays and the number of associated phases for the false events. No events with more than three defining phases were false.

ARCESS	FINESA	NORESS
12	45	8

Table 7.5.8. Distribution of detecting arrays for false one-array events.

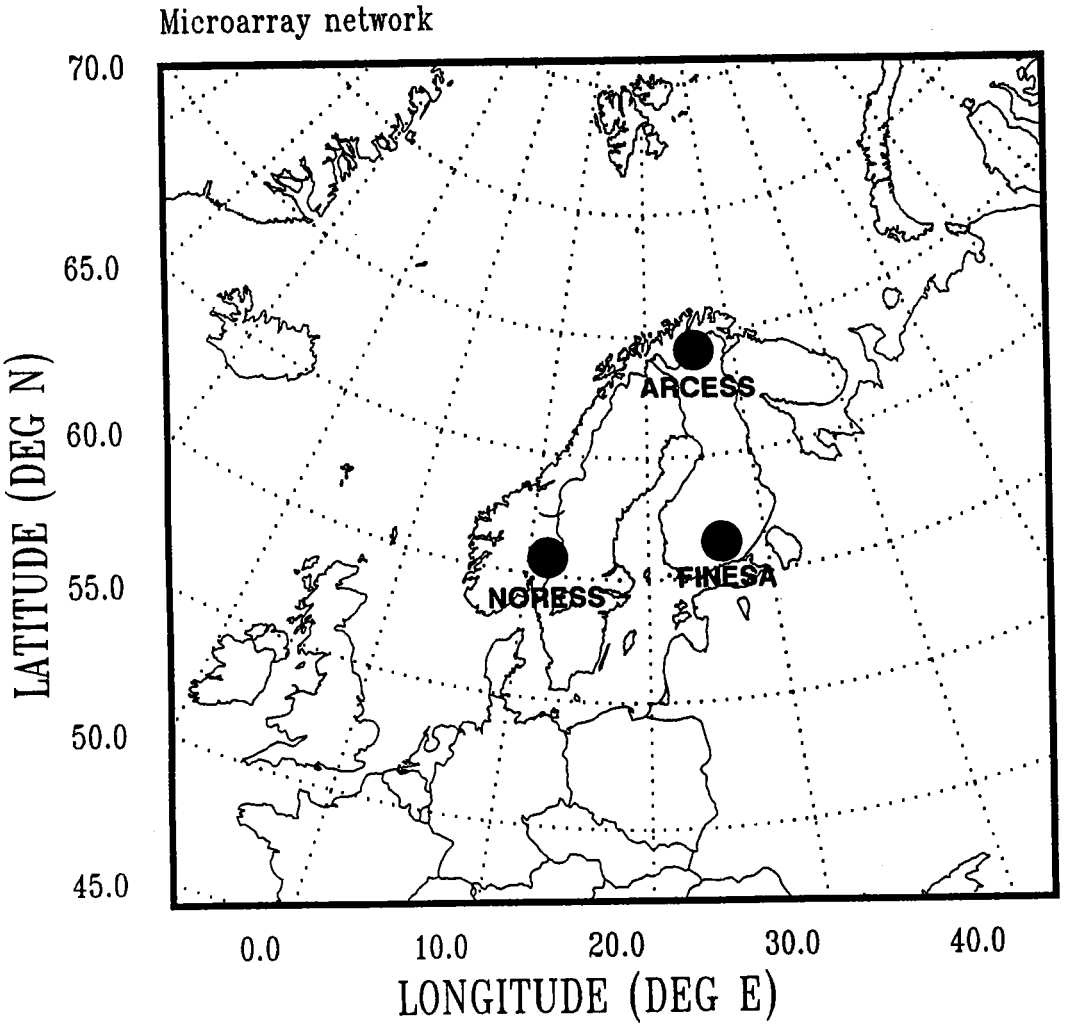

Fig. 7.5.1. Map showing the location of the three Fennoscandian arrays (ARCESS, FINESA and NORESS). The microarray configurations analyzed in this paper are subsets of these arrays.

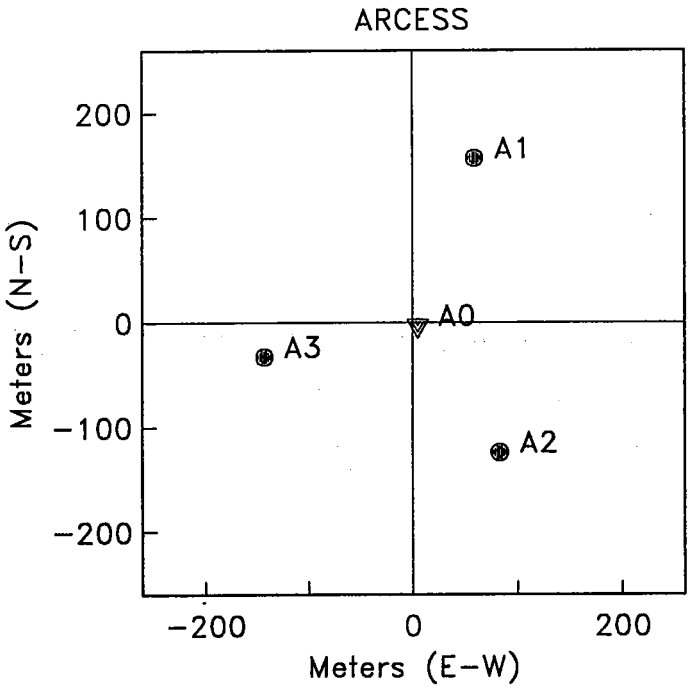

Fig. 7.5.2. This figure gives the locations of the sensors of the ARCESS microarray. The vertical-component sensors are indicated by filled circles, whereas the filled delta symbol represent the 3-component sensor.

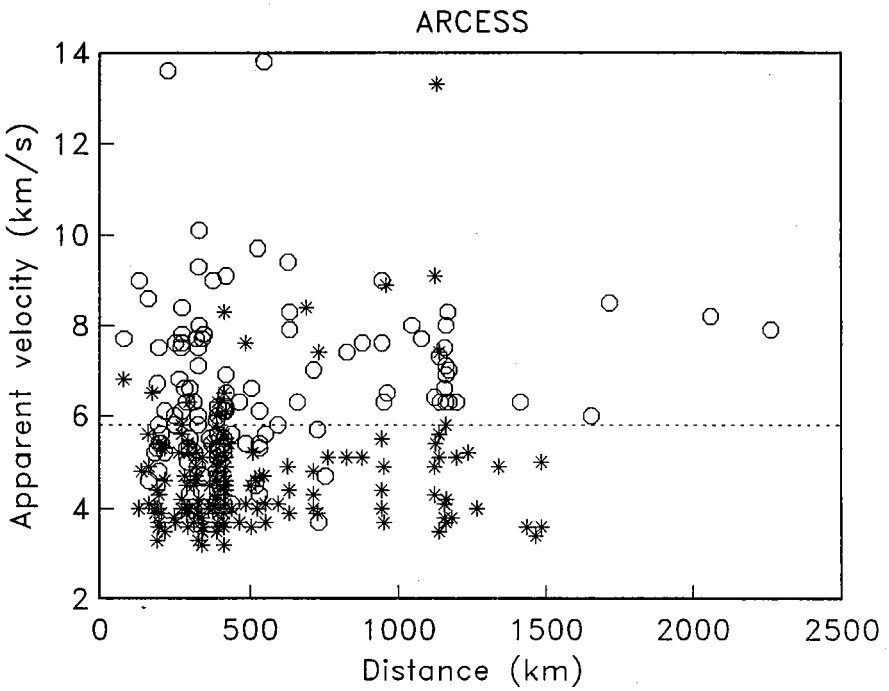

Fig. 7.5.3. Estimated apparent velocities from applying broadband f-k analysis to the vertical components of the ARCESS microarray for *P* phases (circles) and *S* phases (asterisks). An apparent velocity of 5.8 km/s (dashed line) has been used to classify the phases as *P* or *S*. The success rate is 79.2%.

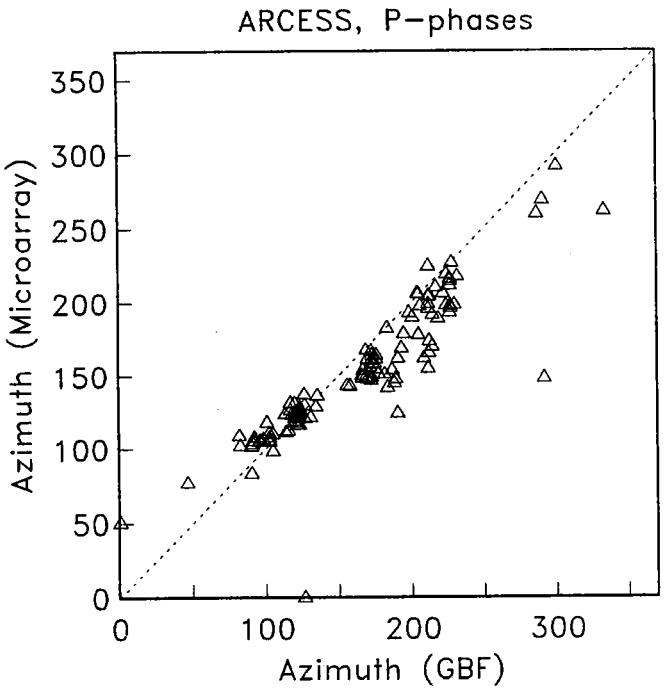

Fig. 7.5.4. Comparison of estimated azimuths of *P* phases using the full ARCESS array and the four vertical components of the ARCESS microarray. The median difference is 10.4°.

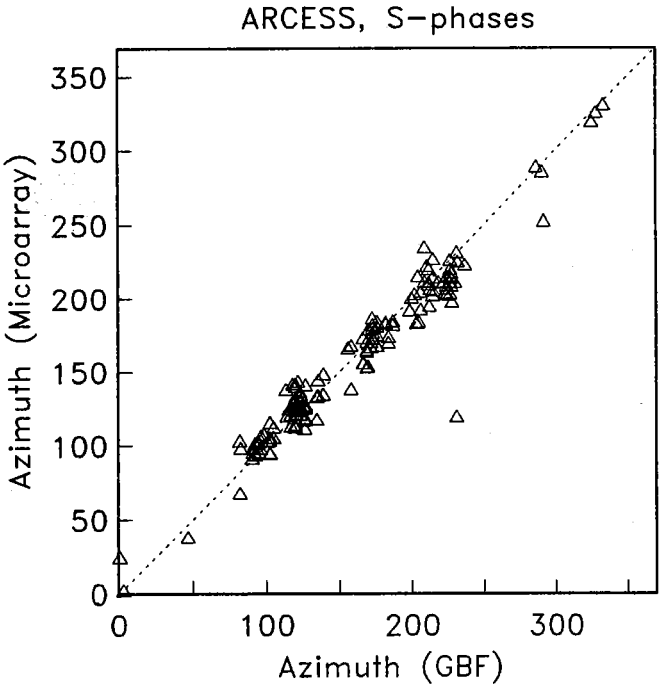

Fig. 7.5.5. Comparison of estimated azimuths of *S* phases using the full ARCESS array and the four vertical components of the ARCESS microarray. The median difference is 6.8°.

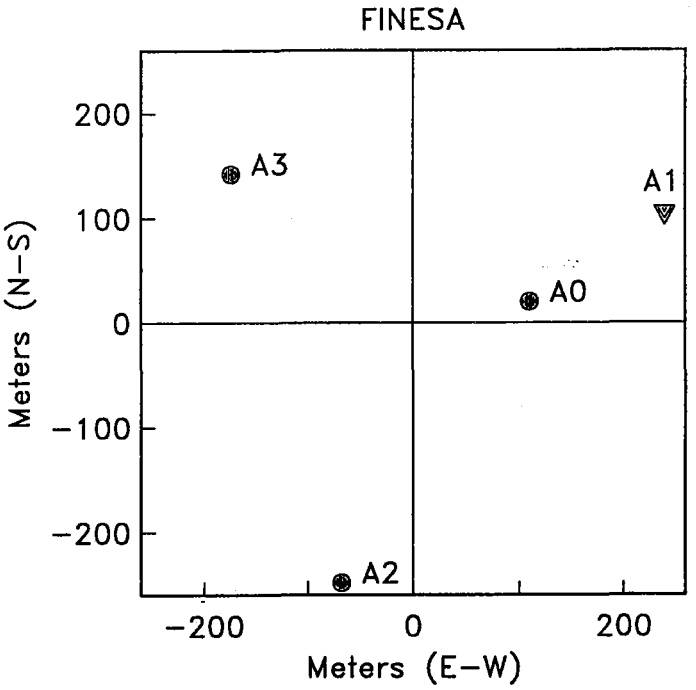

Fig. 7.5.6. This figure gives the locations of the sensors of the FINESA microarray. The vertical-component sensors are indicated by filled circles, whereas the filled delta symbol represent the 3-component sensor.

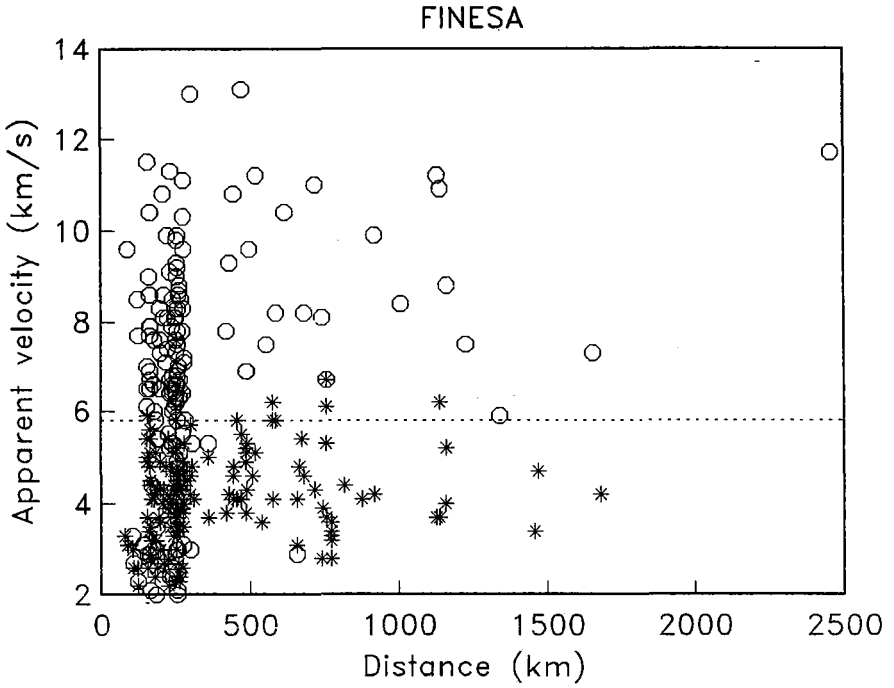

Fig. 7.5.7. Estimated apparent velocities from applying broadband f-k analysis to the vertical components of the FINESA microarray for *P* phases (circles) and *S* phases (asterisks). An apparent velocity of 5.8 km/s (dashed line) has been used to classify the phases as *P* or *S*. The success rate is 78.6%.

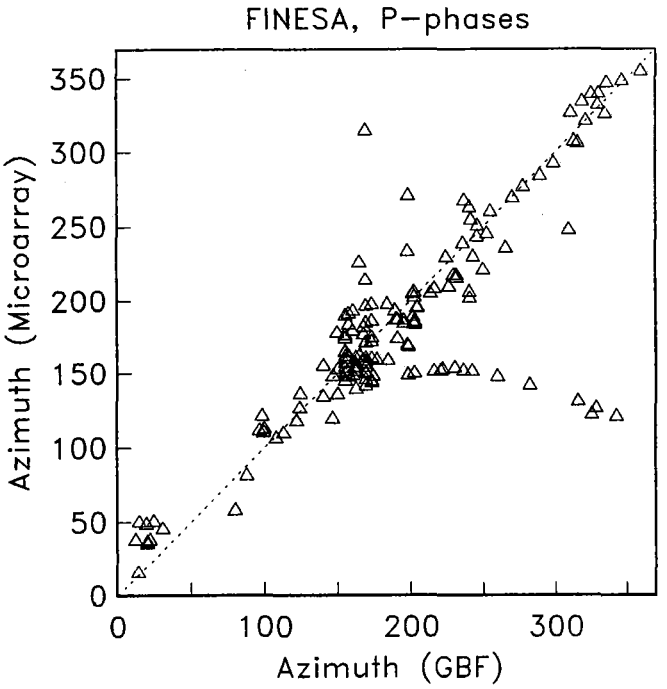

Fig. 7.5.8. Comparison of estimated azimuths of *P* phases using the full FINESA array and the four vertical components of the FINESA microarray. The median difference is 13.4°. Due to the large aperture of the FINESA microarray in comparison with the ARCESS microarray (see Figs. 7.5.2 and 7.5.6) there were some problems with lack of coherency and spatial aliasing at high frequencies. This is the reason for the apparent alignment of *P*-wave azimuth estimates at about 150°.

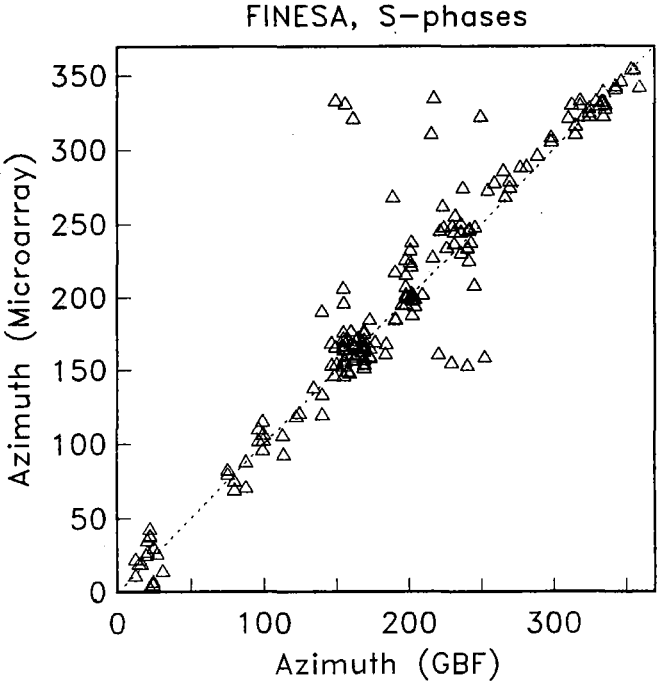

Fig. 7.5.9. Comparison of estimated azimuths of *S* phases using the full FINESA array and the four vertical components of the FINESA microarray. The median difference is 8.5°.

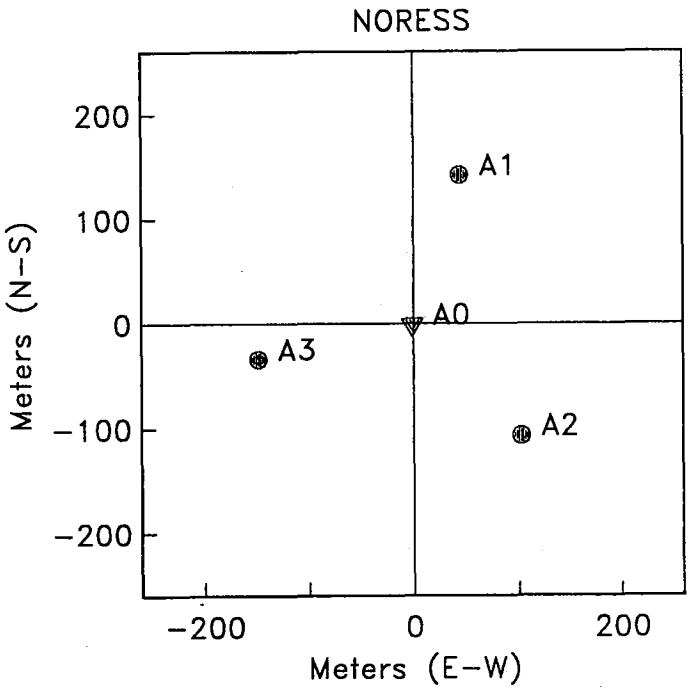

Fig. 7.5.10. This figure gives the locations of the sensors of the NORESS microarray. The vertical-component sensors are indicated by filled circles, whereas the filled delta symbol represent the 3-component sensor.

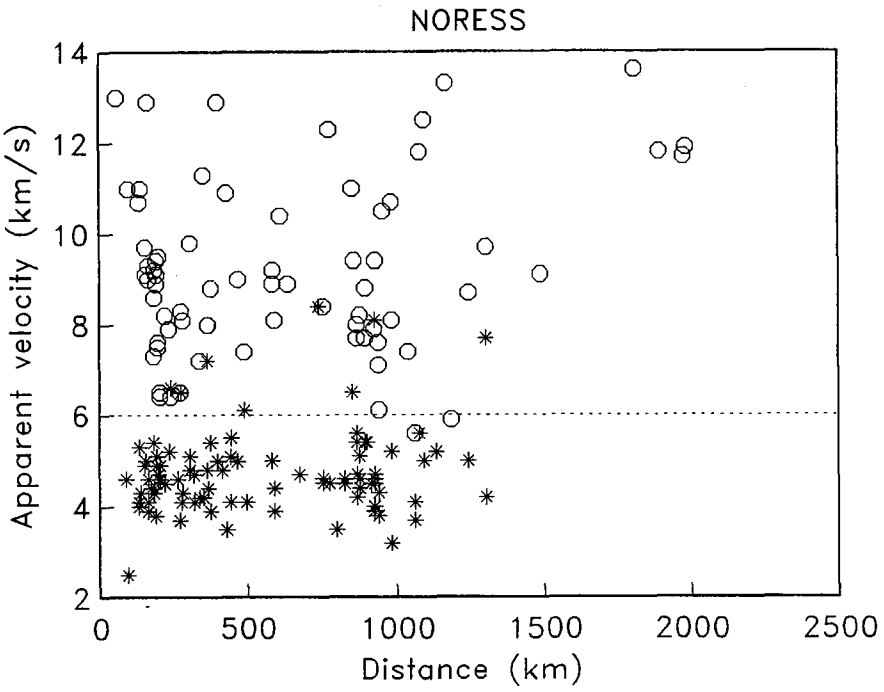

Fig. 7.5.11. Estimated apparent velocities from applying broadband f-k analysis to the vertical components of the NORESS microarray for *P* phases (circles) and *S* phases (asterisks). An apparent velocity of 5.8 km/s (dashed line) has been used to classify the phases as *P* or *S*. The success rate is 93.3%.

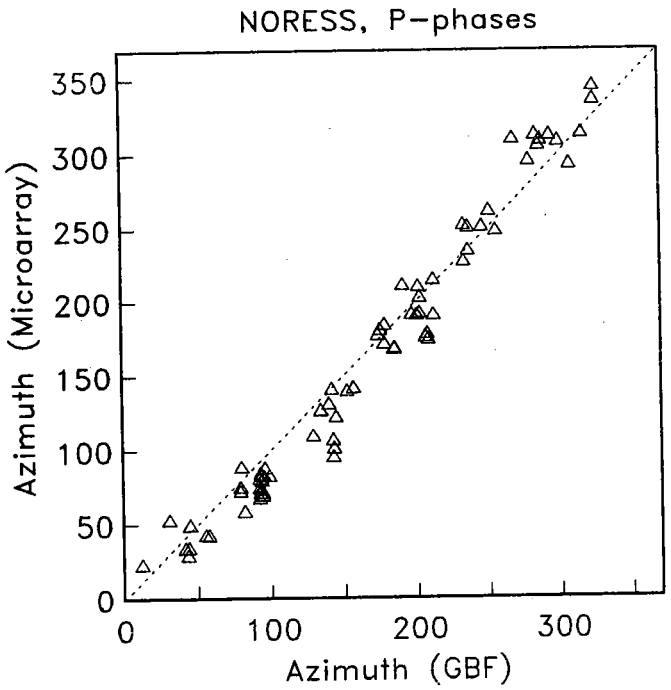

Fig. 7.5.12. Comparison of estimated azimuths of *P* phases using the full NORESS array and the four vertical components of the NORESS microarray. The median difference is 14.0°.

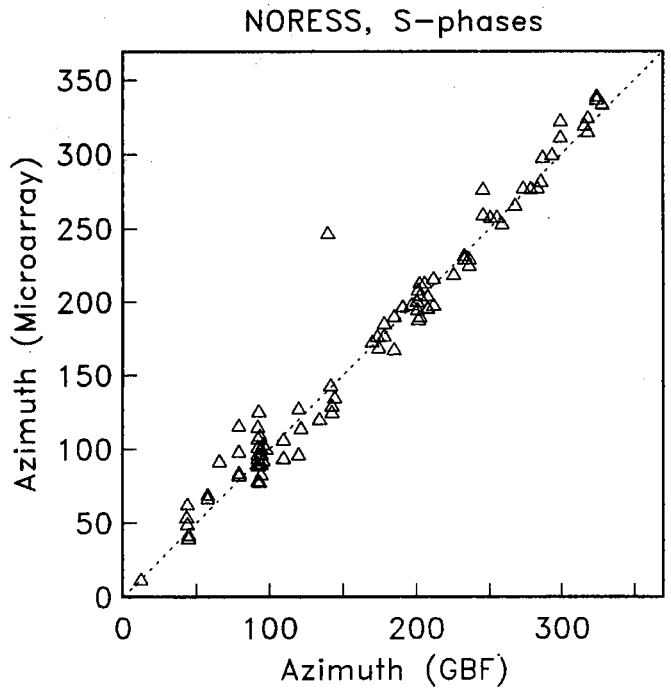

Fig. 7.5.13. Comparison of estimated azimuths of phases using the full NORESS array and the four vertical components of the NORESS microarray. The median difference is 6.5°.

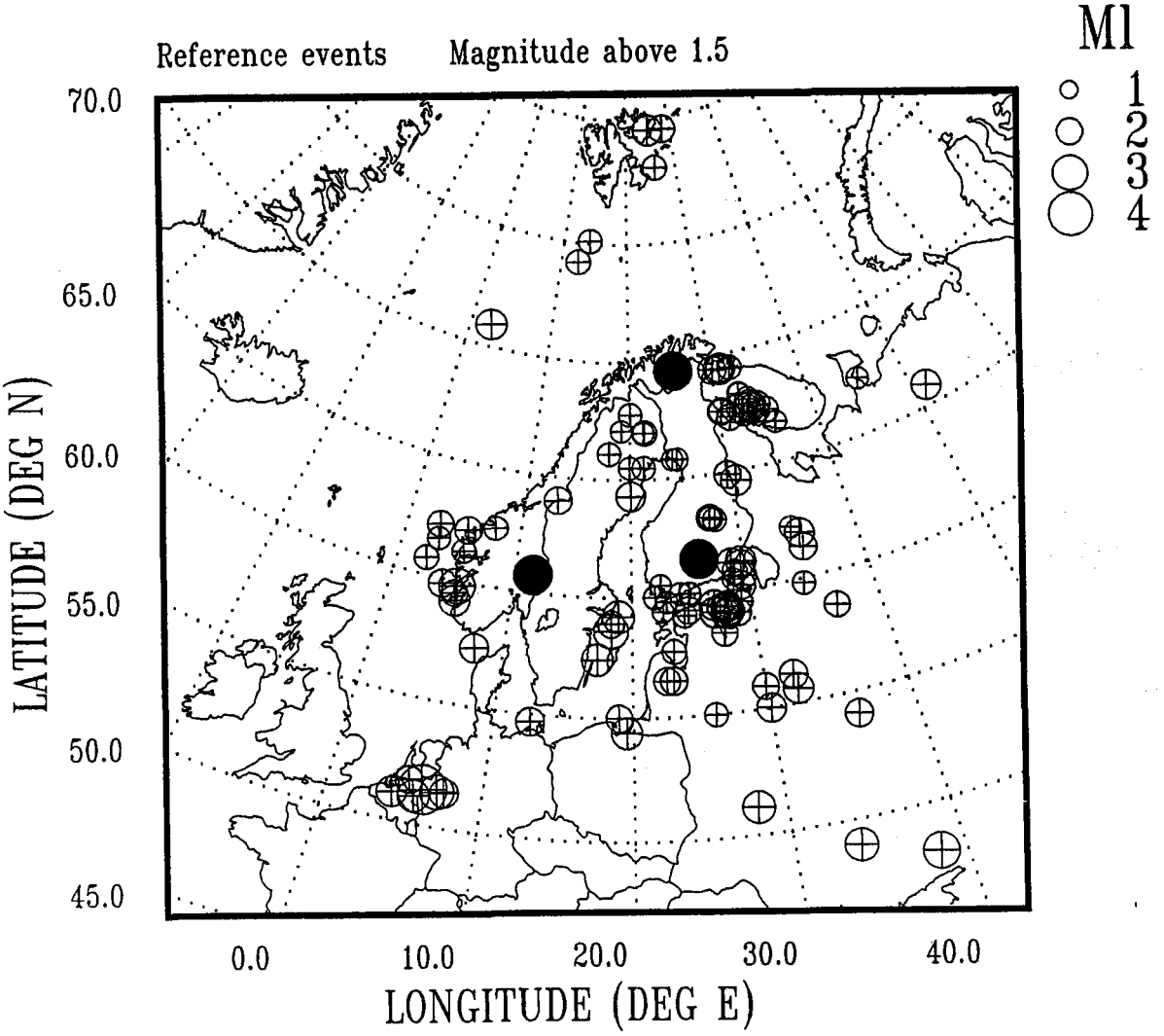

Fig. 7.5.14. Map with reference events with magnitude above 1.5. Note the large number of events (mining explosions) on the Kola peninsula and in Estonia.

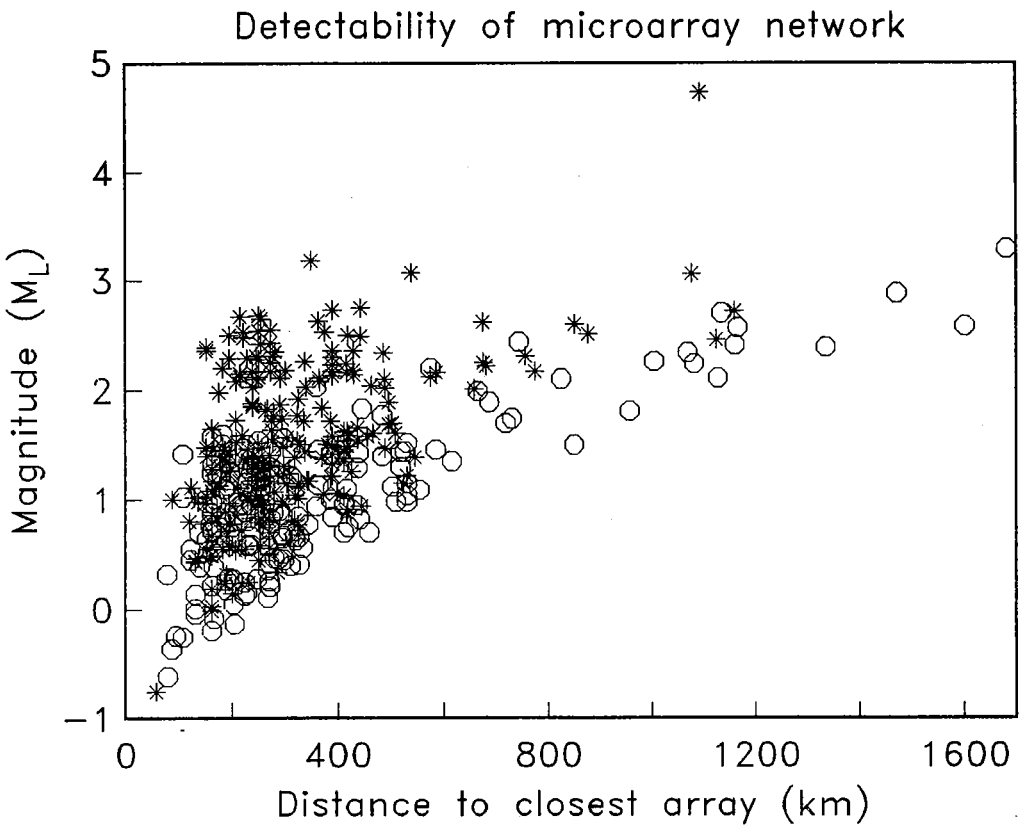

Fig. 7.5.15. Magnitude of reference events versus distance to the closest array. Events found after GBF processing of the microarray network are marked by stars, whereas missed events are marked by circles.

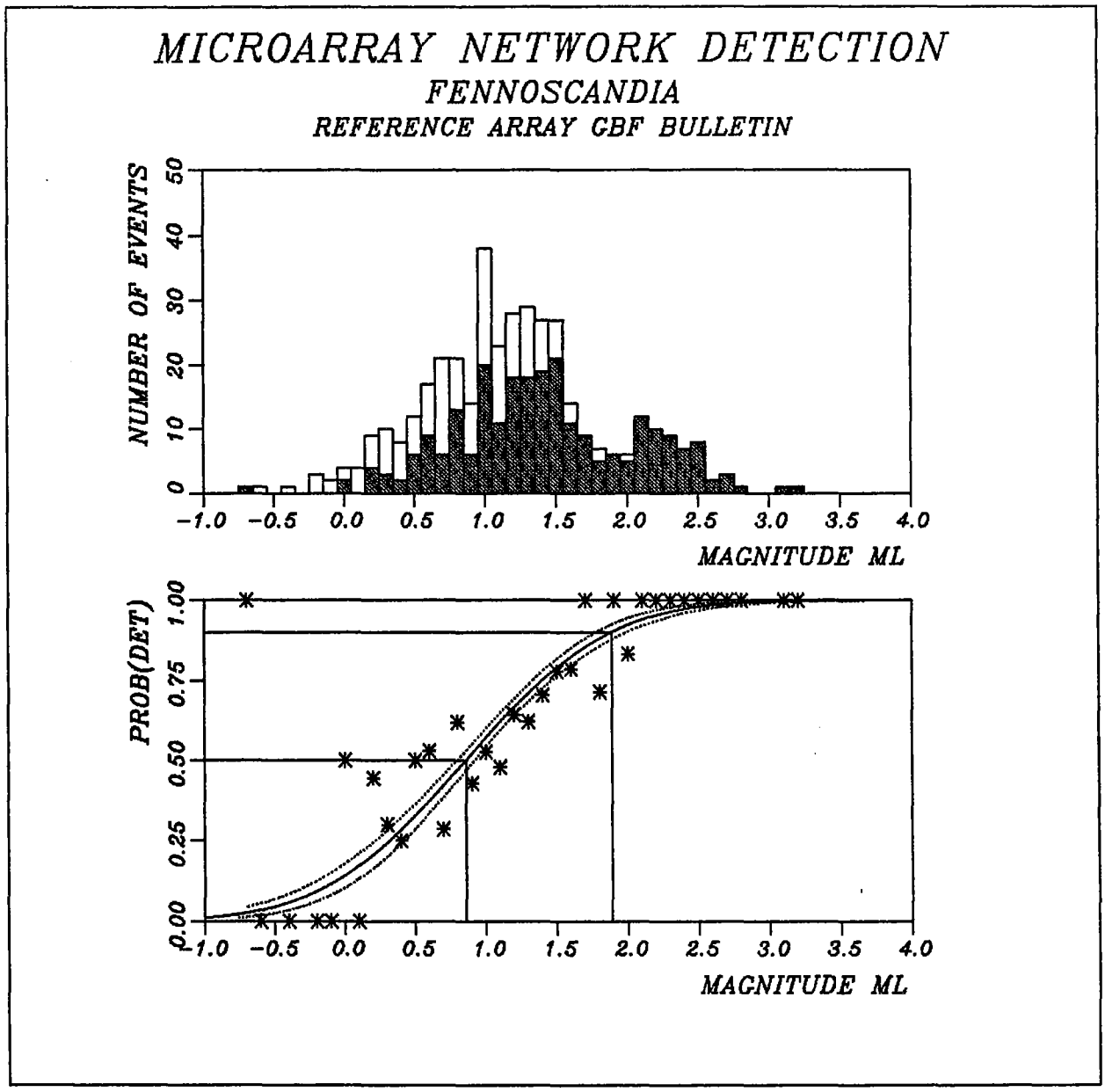

Fig. 7.5.16. Maximum likelihood detectability estimation of the microarray network for Fennoscandia-NW Russia using the GBF bulletin as a reference. The upper half shows the reference set and the number of events found by the microarray network for each magnitude. The lower half shows the maximum likelihood detectability curve and its confidence limits. The actual percentage of detected events at each magnitude is also shown.

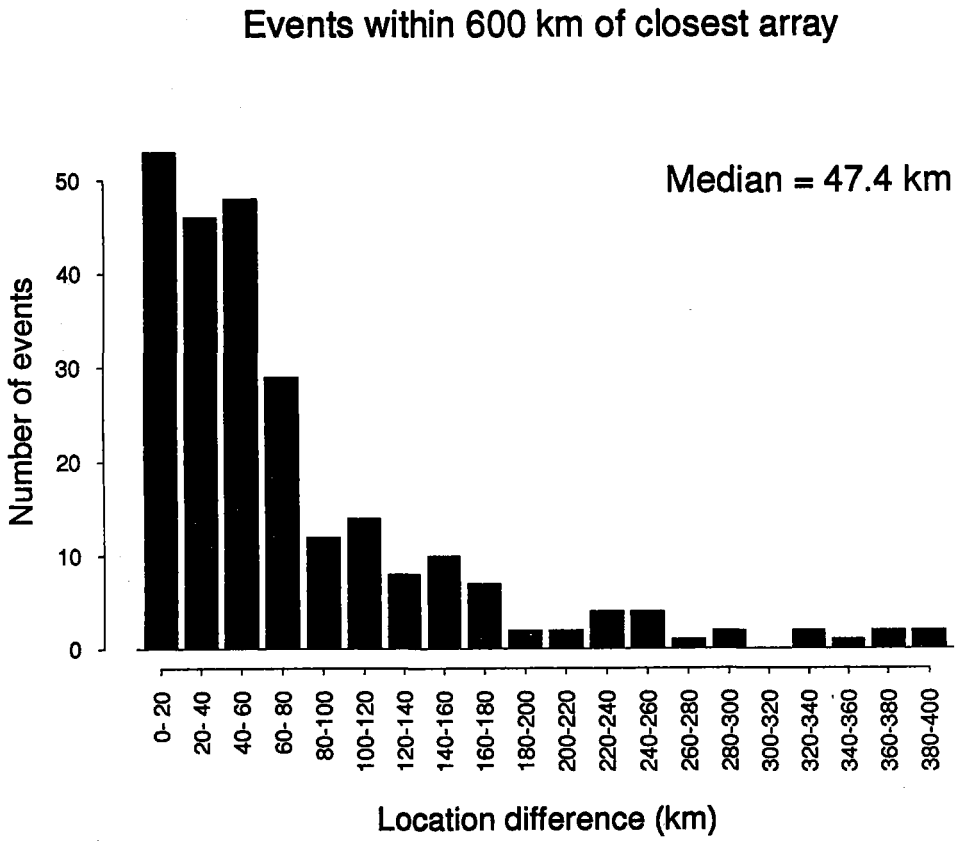

Fig. 7.5.17. This histogram shows the location difference between the microarray network and the full array network for the 249 events located within 600 km of the closest array. The median difference of the population is 47.4 km.